



# Stable isotopes of tree rings reveal seasonal-to-decadal patterns during the emergence of a megadrought in the Southwestern US

Paul Szejner<sup>1,2</sup> · Soumaya Belmecheri<sup>2</sup> · Flurin Babst<sup>2,3,4</sup> · William E. Wright<sup>2</sup> · David C. Frank<sup>2</sup> · Jia Hu<sup>2,4</sup> · Russell K. Monson<sup>2,5</sup>

Received: 17 July 2020 / Accepted: 8 April 2021

© The Author(s), under exclusive licence to Springer-Verlag GmbH Germany, part of Springer Nature 2021

## Abstract

Recent evidence has revealed the emergence of a megadrought in southwestern North America since 2000. Megadroughts extend for at least 2 decades, making it challenging to identify such events until they are well established. Here, we examined tree-ring growth and stable isotope ratios in *Pinus ponderosa* at its driest niche edge to investigate whether trees growing near their aridity limit were sensitive to the megadrought climatic pre-conditions, and were capable of informing predictive efforts. During the decade before the megadrought, trees in four populations revealed increases in the cellulose  $\delta^{13}\text{C}$  content of earlywood, latewood, and false latewood, which, based on past studies are correlated with increased intrinsic water-use efficiency. However, radial growth and cellulose  $\delta^{18}\text{O}$  were not sensitive to pre-megadrought conditions. During the 2 decades preceding the megadrought, at all four sites, the changes in  $\delta^{13}\text{C}$  were caused by the high sensitivity of needle carbon and water exchange to drought trends in key winter months, and for three of the four sites during crucial summer months. Such pre-megadrought physiological sensitivity appears to be unique for trees near their arid range limit, as similar patterns were not observed in trees in ten reference sites located along a latitudinal gradient in the same megadrought domain, despite similar drying trends. Our results reveal the utility of tree-ring  $\delta^{13}\text{C}$  to reconstruct spatiotemporal patterns during the organizational phase of a megadrought, demonstrating that trees near the arid boundaries of a species' distribution might be useful in the early detection of long-lasting droughts.

**Keywords** Multidecadal · Warming · Hot drought · Intrinsic water-use efficiency · Vapor pressure deficit

## Introduction

Alternations of seasonal wet and dry phases are captured in the structure and composition of tree rings and are particularly relevant to investigations of coupled patterns in the water and carbon cycles of montane forests in western North America (Leavitt et al. 2002, 2011; Szejner et al. 2016, 2020a; Belmecheri et al. 2018). In the Southwestern United States (US), early-season forest productivity is driven by snowmelt water, followed by a dry and less-productive period during the late-spring and early summer (Monson et al. 2002; Knowles et al. 2018). In the driest sites, a mid-summer hyper-arid period may accompany extremely hot weather, bringing forest productivity to a near halt (Knowles et al. 2020). Later in the summer, when conditions become less arid in response to convective storms, productivity rates generally recover (Szejner et al. 2016, 2018, 2020a). These alternating seasonal influences provide distinct intra-annual climatic signals in the earlywood and latewood rings

---

Communicated by Christiane Roscher .

✉ Paul Szejner  
szejner@geologia.una.mx

<sup>1</sup> Instituto de Geología, Universidad Nacional Autónoma de México, 04510 Mexico City, Mexico

<sup>2</sup> Laboratory of Tree-Ring Research, University of Arizona, 1215 E Lowell St, Tucson, AZ 85721, USA

<sup>3</sup> W. Szafer Institute of Botany, Polish Academy of Science, ul. Lubicz 46, 31-512 Krakow, Poland

<sup>4</sup> School of Natural Resources and the Environment, University of Arizona, 1064 E. Lowell St., Tucson, AZ 85721, USA

<sup>5</sup> Department of Ecology and Evolutionary Biology, University of Arizona, Tucson, AZ 85721, USA

of many coniferous trees, especially those in the Pinaceae (Leavitt et al. 2002; Szejner et al. 2016; Belmecheri et al. 2018). This has made it possible to reconstruct seasonal variation in hydroclimate and carbon-climate relations in the Southwestern US across multiple decades of climate variation (Leavitt et al. 2002, 2011; Monson et al. 2018; Szejner et al. 2020b).

Recent investigations of hydroclimate trends in the Southwestern US have shown progressively increased aridity (Cook and Seager 2013). Data from tree ring records of stable isotope composition and growth, as well as model hindcasts, have shown evidence of a change in the pace and magnitude of cumulative droughts in the Western US, coalescing into what is formally described as a contemporary megadrought, with an approximate start date of 2000 (Szejner et al. 2020a; Williams et al. 2020). Megadroughts are defined as those droughts persisting for at least 2 decades. These types of long-term droughts have occurred in the Western US in the past 2000 years, but not since at least the late 1500 s (Woodhouse and Overpeck 1998; Cook et al. 1999, 2010; Stahle et al. 2020). The current megadrought's persistence is caused by a combination of decadal-scale oscillations in Eastern Pacific sea surface temperatures and associated shifts in precipitation patterns, and enhanced regional terrestrial evaporation, most likely due to anthropogenic climate warming (Williams et al. 2020). The extreme drought conditions have been reported for both winter and summer precipitation, along with drier atmospheric humidity, across a broad region in the Western US (Szejner et al. 2020a). The fact that we had to wait two decades to confidently designate this anomaly as a megadrought speaks to our lack of efficient prognostic indicators and models. It is unknown how temporal and spatial patterns in local droughts cumulate and coalesce over time to form regional events, like megadroughts, and this lack of knowledge hampers our predictive capabilities. In search of ways to enhance these capabilities, we studied the isotopic composition and growth of tree rings in *P. ponderosa* trees as a means to detect changes in regional drought regimes (Fritts 1976; Leavitt et al. 2002; Griffin et al. 2011; Szejner et al. 2016; 2020a). Our specific aim was to obtain insight into how ponderosa pine (*P. ponderosa*) trees, growing at the southern, most arid part of the species' range, have responded to drought in the decades preceding and during the current Southwestern US megadrought.

The seasonal and phenological patterns in cambial activity in *P. ponderosa* in the Southwestern US have been well resolved in past studies (Budelsky 1969; Fritts et al. 1991; Morino et al. 2021). After winter dormancy, cambial growth begins by early-to-mid April. Growth rates are highest during the early growing season and decrease progressively toward summer as precipitation decreases, soil moisture reserves become depleted, and atmospheric vapor pressure

deficit (VPD) increases. In late spring and early summer, a hyper-arid period often occurs, which causes a sharp reduction in cambial growth, correlated with decreases in needle transpiration and photosynthesis (Budelsky 1969; Knowles et al. 2020; Morino et al. 2021). The result of this regular seasonal drought is often visible in the boles of *P. ponderosa* as a narrow band of small diameter tracheids, known as an intra-annual density fluctuation (IADF) or 'false late-wood band'. The IADF can be used as a wood anatomical marker to distinguish the bimodal (winter and summer) phases of seasonal precipitation (Griffin et al. 2011; Morino et al. 2021). IADFs consistently occur in the annual rings of trees from mid-altitude montane forests from Mediterranean and semi-arid climates, and have been used in the past to distinguish spring growth from summer growth (De Micco et al. 2007; Battipaglia et al. 2016; Zalloni et al. 2016; Acosta-Hernández et al. 2019; Pacheco et al. 2019). Following the early-summer hyper-arid period, usually by the first week of July (Higgins et al. 1997), the North American Monsoon (NAM) climate system brings regular convective rain storms to the Southwestern US, and *P. ponderosa* trees in montane ecosystems resume their cambial activity and growth (Budelsky 1969; Morino et al. 2021). In this case, the smaller cells produced in the IADFs are followed by the larger cells of latewood, thereby providing a distinct anatomical boundary that marks the end of growth during the hyper-arid season.

In addition to studying intra-annual biomass growth patterns through ring-width increments, we examined the carbon and oxygen stable isotope compositions of cellulose, which were used as physiological proxies to assess leaf intrinsic water-use efficiency (iWUE, in the case of  $\delta^{13}\text{C}$ ) and potential transpiration rate (in the case of  $\delta^{18}\text{O}$ ). iWUE is defined as the rate of carbon acquired through photosynthesis ( $A$ ) divided by the rate of stomatal conductance to water vapor ( $g_s$ ), and thus serves as a useful measure of the quantitative coupling between potential carbon and water exchanges at the leaf scale (Farquhar et al. 1982; Francey and Farquhar 1982; Ehleringer and Cerling 1995; Gessler et al. 2014; Frank et al. 2015). Using a diffusive-analog model for the condition of a well-mixed atmosphere with negligible needle-surface boundary layers, we can state:  $iWUE \sim A/g_s \sim (c_a - c_i)/1.6$ , where  $c_i$  is the intercellular  $\text{CO}_2$  concentration of the needle,  $c_a$  is the atmospheric  $\text{CO}_2$  concentration, and 1.6 is the ratio of the diffusivities of  $\text{H}_2\text{O}$  and  $\text{CO}_2$  in air. Relations between the  $\delta^{13}\text{C}$  of photosynthate and iWUE are mechanistically connected by the variability of the  $\text{CO}_2$  concentrations ( $c_i/c_a$ ) (Farquhar et al. 1982). The relationship between  $\delta^{13}\text{C}$  of the tree-ring cellulose and iWUE can be more complex due to post-assimilation fractionations, especially in sugars as they are loaded into the phloem for transport (Gessler et al. 2014). Nonetheless, the tree-ring  $\delta^{13}\text{C}$  record appears to retain a relatively

accurate climate signal that generally reflects fluctuations in iWUE in response to precipitation and atmospheric VPD (Francey and Farquhar 1982; Gessler et al. 2014; Frank et al. 2015; Szejner et al. 2016). The  $\delta^{18}\text{O}$  of wood cellulose has also been used to reconstruct atmospheric aridity, but it is less reliable in its dependency on climate compared to  $\delta^{13}\text{C}$ , because  $\delta^{18}\text{O}$  is influenced by three variables: (1) temporal variability in the isotopic content of the water sources used by plants, (2) isotopic enrichment (in transpiring leaves) driven by VPD, and (3) the percentage of post-assimilation oxygen isotope exchange before and during cellulose synthesis (Roden et al. 2000; Treydte et al. 2014; Szejner et al. 2020b). Collectively, assessing the relative importance of these physiological features provides insights into better understand the seasonal and interannual variations in local droughts and their influence on tree ecophysiology.

In this study, we aimed to achieve a deeper understanding of how drought affects trees across multiple time scales prior to and during an emerging megadrought in four populations of *P. ponderosa* located across a longitudinal transect at the southern, most arid distribution limit of the species. The longitudinal transect introduced an additional climate variable into the analysis, as it stretched across a gradient in the relative distributions of winter and summer precipitation. We assessed nearly equal decadal-scale periods immediately prior to, and after, the onset of the megadrought in 2000. Specifically, we addressed two questions: (1) What were the site-dependent differences in tree-ring growth and stable isotope responses before and during the emergent megadrought? (2) If there was evidence of megadrought development in ring growth and stable isotope composition prior to 2000, were there key times during the growing season when these signals were most obvious? By addressing these questions, we aimed to explore if local influences of drought on tree ecophysiology in a widely distributed montane species, near the arid limit of its existence and where drought sensitivity may be relatively high, provide early indications of the impending megadrought.

## Methods

### Study sites

The four study sites are situated along a longitudinal transect stretching east-to-west across the northern reach of the NAM domain (Figs. 1 and 2). Sampled trees were growing in the Santa Catalina Mountains (HEL) and Pinalenos Mountains (UAC) in southern Arizona, and the Gila Mountains (GFP) and Sacramento Mountains (CCP) in southern New Mexico (Table 1). Although the sites cover a significant east-to-west gradient (across  $\sim 5^\circ$  of longitude), they are within  $0.5^\circ$  of the same latitude. The sites are characterized

by variable proportions of winter versus summer precipitation. Due to their proximity to the Gulf of Mexico, seasonal initiation of NAM precipitation begins earlier ( $\sim 15$  June–5 July) in the New Mexico sites, compared to the Arizona sites ( $\sim 5$ –15 July). The selected trees at each of the four sites were between 70 and 100 years old, and initial cores revealed that they exhibited IADF bands in at least 65% of their annual rings. The study time frame for climate analysis was 1980–2019, whereas the study time frame for isotope analysis was 1985–2014. Thus, our study covers two decades before and during the megadrought for climate characterization, but only 1.5 decades before and during for isotope characterization.

We compared tree responses in the four study sites with those in ten other sites that extend across the latitudinal extent of the NAM geographic domain and were extensively studied previously (Szejner et al. 2020a). This provided us with a set of reference sites to serve as controls in addressing our hypothesis that trees at the southern, most arid location of the four primary study sites, exhibit unique responses to the emergent megadrought.

### Tree-ring width and blue-light reflectance parameters

We collected two increment cores to the pith of 20 mature trees at each site. A subset of three to five trees was selected for isotopic analyses based on the criterion of exhibiting an IADF in almost every year. In the first step of sample preparation, we extracted the resin from all samples in a Soxhlet apparatus containing 99% ethanol for 20 h to enable blue-light intensity measurements as a proxy of wood density (Campbell et al. 2011). We then followed standard dendrochronological procedures to prepare the cores for radial tree growth measurements (Stokes and Smiley 1996), including drying, sanding, and polishing a horizontal surface perpendicular to the fiber direction and down to 15  $\mu\text{m}$  grit.

All samples were visually dated under a light microscope. Then, each sample was scanned using an Epson Expression 10,000 XL flatbed scanner at a spatial resolution of 2400 dpi. Radial growth parameters were extracted from the resulting digital images using the WinDendro software (Regents Instruments Inc) for earlywood width (EW), latewood width (LW), and total ring width (TRW). The correct assignment of each ring to a calendar year was again visually and statistically verified (“cross-dating”) using the COFECHA software (Holmes 1992). IADF density characteristics were determined using the blue channel of a standard red–green–blue digital image, which is sensitive to the lignin content of wood cell walls and yields blue pixel values that reflect density changes throughout the ring. IADFs appeared as a peak of high density (i.e., low blue reflectance). Following Babst et al.

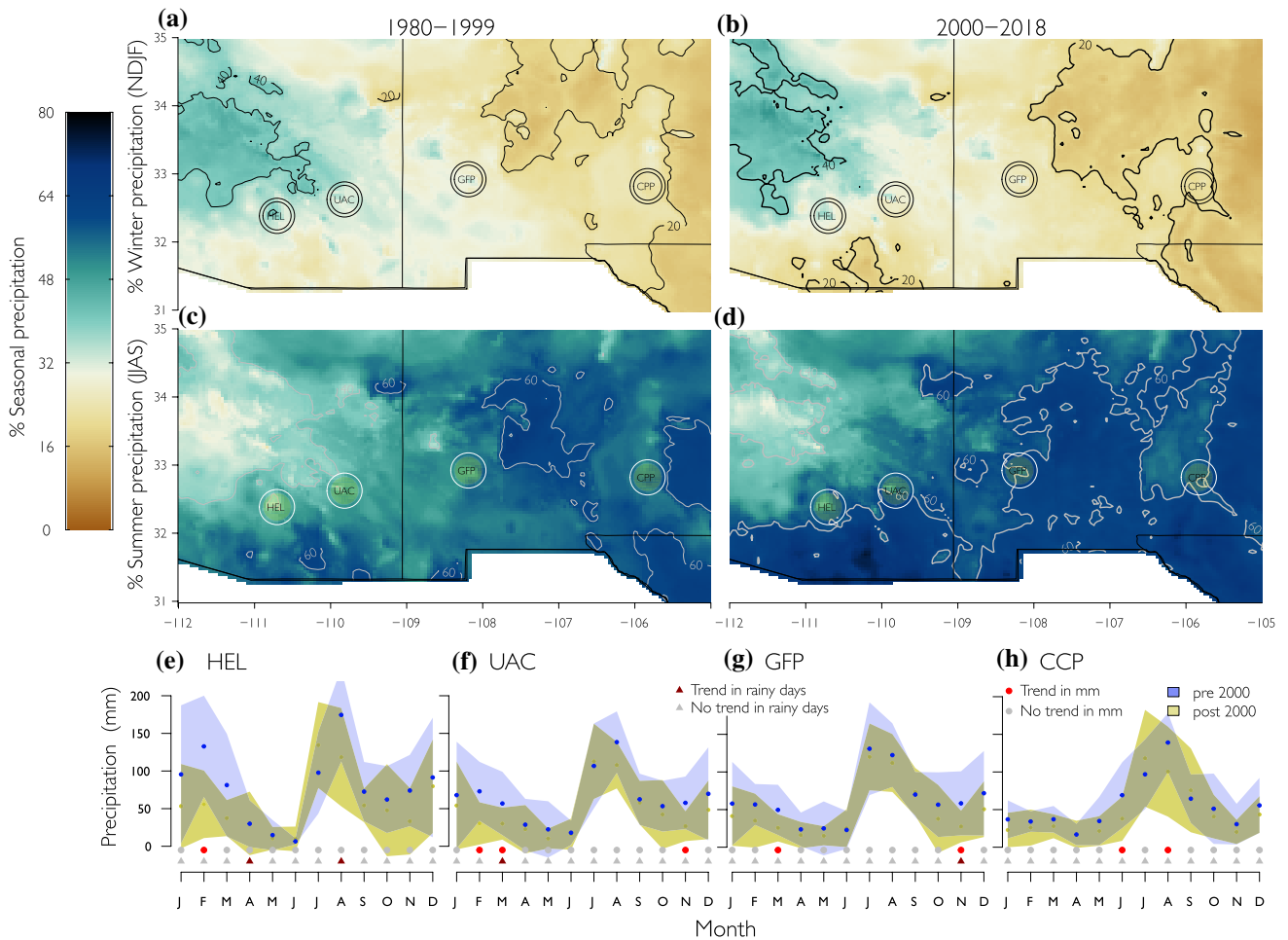


**Fig. 1** Precipitation seasonality for each study site for the period before and after the onset of the megadrought in 2000 CE. Regional percentages of annual total precipitation during the (a, b) winter and (c, d) summer seasons. The four study sites are indicated with circled acronyms. e–h Monthly precipitation (mm) for each site in pre- and post-megadrought onset (pre: 1980–1999 in blue and post: 2000–2019 in yellow). Data were taken from daily values from the

PRISM database. Red dots show months with a significant negative trend ( $P < 0.05$ ) in precipitation. Brown triangles show months with a significant negative trend ( $P < 0.05$ ) in the number of rainy days with daily precipitation greater than 3 mm from 1980 to 2019. Grey dots and triangles show months with no significant trends in precipitation or number of rainy days

(2016), we used a peak-detection algorithm from the *pracma* package in R (Borchers 2019) to locate and characterize the peak. The derived parameters included peak position within the ring (relative and absolute), width, height, and area.

We aligned the relative seasonality of different portions of each annual ring using the IADF as a reference point. The first seasonal domain indicates growth during the spring (PRE-IADF) which reflects two portions of earlywood (EW1 and EW2). The second domain is the growth during the early-summer hyper-arid period (IADF), which reflects the false latewood (FLW), and the third domain aligns with growth during the summer monsoon season (POST-IADF) which reflects summer

wood (SW) and latewood (LW) (see Babst et al. 2016; Belmecheri et al. 2018).

### Intra-annual stable isotope measurements

For isotopic analyses, growth rings from 1985 to 2014 were subdivided into the five consecutive sections listed above and described previously (Belmecheri et al. 2018). Based on observations of anatomical features related to cell size, the five designated sections were separated from each ring using a scalpel: two equal-width sections on the PRE-IADF, called earlywood 1 (EW1) and earlywood 2 (EW2); one section of the IADF; and two sections in the POST-IADF section, called summerwood (SW) and latewood (LW) sections.

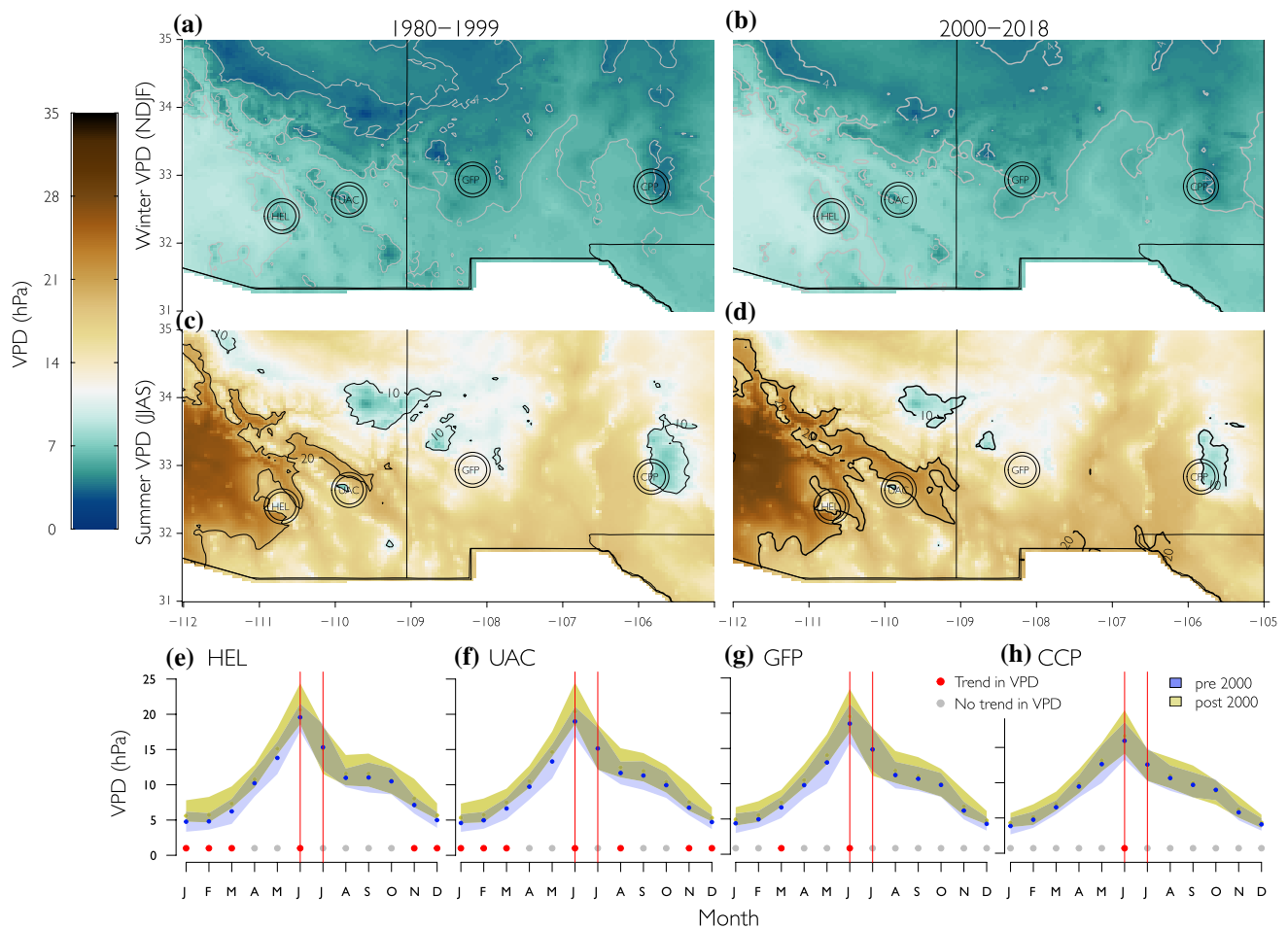


**Fig. 2** Atmospheric vapor pressure deficit (VPD) for each study site for the period before and after the onset of the megadrought in 2000 CE. The symbols are the same as those presented in Fig. 1. The val-

ues of VPD correspond to the average monthly VPD values. Red dots show months with a significant positive trend ( $P < 0.05$ ) in VPD from 1980 to 2019

**Table 1** Site characteristics organized from the west (top) to east (bottom)

Site	Latitude	Longitude	Elevation (masl)	NAM onset
Santa Catalina Mtns (HEL)	32.40	- 110.70	2230	July 1–July 15
Pinalaños Mtns (UAC)	32.64	- 109.81	2050	July 1–July 15
Gilas Mtns (GFP)	32.94	- 108.18	2311	June 15–July 5
Sacramento Mtns (CCP)	32.84	- 105.83	2225	June 15–July 5

HEL and UAC are located in the state of Arizona, GFP, and CCP are located in the state of New Mexico. Average monsoon start date and proportion of winter versus summer precipitation were determined from the PRISM climate database

NAM North American monsoon, *masl* meters above sea level

Two exceptions to this sampling design were (a) years where the IADF position was relatively close to the previous ring boundary ( $n = 10$ ), in which case, we only distinguished one EW section and (b) years where the IADF position was close to the LW  $n = 12$  in which case no SW was used. For those occasional years without an IADF ( $n = 4$ ), the ring was either

analyzed in its entirety or divided into two or three equal parts, depending on the EW width.

Wood samples were ground to pass a 20-mesh filter, and  $\alpha$ -cellulose was extracted from each sample following Green (1963), as modified by Leavitt and Danzer (1993), and with the addition of a NaOH extraction step to remove hemicelluloses, followed by sonication to ensure homogeneity

(Laumer et al. 2009). Cellulose samples were analyzed for carbon and oxygen isotope ratios ( $\delta^{13}\text{C}_{\text{cel}}$  and  $\delta^{18}\text{O}_{\text{cel}}$ , respectively) using isotope–ratio mass spectrometry at the University of Maryland, following the protocol described in Evans et al. (2006). The overall precision values for the corrected data, based on replicate standard analyses, are 0.11‰ for  $\delta^{13}\text{C}$  and 0.24‰ for  $\delta^{18}\text{O}$ . The  $\delta^{13}\text{C}_{\text{cel}}$  values were corrected for the decline of atmospheric  $^{13}\text{C}/^{12}\text{C}$  ratio since the Industrial Revolution, following the procedure described in McCarroll et al. (2009) and using Northern Hemisphere atmospheric  $\text{CO}_2$  concentrations and atmospheric  $\delta^{13}\text{C}$  ratios available from the database of the Mauna Loa observatory in Hawaii (Keeling et al. 2005).

## Data analysis

Using PRISM gridded datasets (PRISM Climate Group 2004), we calculated, on a regional scale, the proportion of precipitation during winter months from November to February (NDJF) and summer months from June to September (JJAS) for the periods prior to and after the onset of the megadrought in 2000 (i.e., 1980–1999, and 2000–2019) (Fig. 1). For the same two periods, we also calculated the mean winter and summer VPD (Fig. 2). We conducted an analysis of decadal-scale trends in precipitation and VPD on the four sites detailed in this study, as well as ten additional sites that were included in a past study (Fig. 3; Szejner et al. 2020a), but have not before now been analyzed for monthly climate trends before and during the megadrought. The ten additional sites, from further north, were used as a contrast with the four new sites at the southern range-limit of the species.

All trends were estimated using a linear regression model with time as the independent variable. We used the slopes from the linear regression and corresponding  $P$  values to assess significance levels among trends, and applied the analysis separately for each month pre- and post-2000. Additionally, using a Mann–Whitney test we assessed the differences between mean annual climate conditions for 1980–1999 (pre-megadrought) and 2000–2019 (megadrought). Because the monthly time series in precipitation and VPD displayed a large degree of variance, we applied a 5-year smoothing spline on each record to reduce inter-annual variability. Using the daily data from PRISM, we quantified the number and temporal trends for rainy days for each month. Additionally, for site versus regional comparison, we assessed the trends from monthly precipitation, VPD and tree response via the principal component analysis from the  $\delta^{13}\text{C}$  tree-ring network, as described in Szejner et al. (2020a). Trends in the tree-ring parameters (RW,  $\delta^{13}\text{C}$ , and  $\delta^{18}\text{O}$ ) were estimated over the 30-year period from 1985 to 2014, the full extent of the records, without any smoothing of the data. For each sub-section of the annual ring, we

assessed the seasonal progression of  $\delta^{13}\text{C}$  and  $\delta^{18}\text{O}$  during the 30-year period. We determined the statistical difference among sub-section mean values for  $\delta^{13}\text{C}$  and  $\delta^{18}\text{O}$  using the Tukey Honest Significant Differences (HSD) applied on the ANOVA test comparing different sections (E1, E2, FLWB, SW, LW) and different climate periods (pre- and post-2000).

## Results

### Seasonal climate patterns at the study sites

Because winter precipitation is delivered from westerly synoptic weather systems, the two westernmost sites, in Arizona (HEL and UAC), receive significantly more of their annual precipitation during the winter (generally between 30 and 40%) (Fig. 1, upper panels). By contrast, the two easternmost sites, in New Mexico (GFP and CCP), receive the majority of their annual precipitation as summer rain from the NAM (~60%), with less than 20% delivered as winter snow. The emergence of the post-2000 megadrought manifested itself as reductions in winter and spring precipitation at all four sites (Fig. 1, lower panels). The date for the onset of the NAM at each site was not affected by the megadrought. The emergence of the megadrought was generally observed as a decrease in precipitation (Fig. 1) and increase in VPD (Fig. 2). The CPP site also showed less reduction in winter precipitation during the megadrought and showed no significant trends in winter precipitation during 1980–2019 (Fig. 1), relative to the other three sites; though, we restate that most (>75%) of the annual precipitation at this site occurs during the summer. The other three sites (HEL, UAC, and GFP) show a decreasing trend ( $P < 0.05$ ) in the amount and number of rainy days during winter and spring for 1980–2019 (Fig. 1). There were statistically significant ( $P < 0.05$ ) differences in the mean annual values of precipitation and VPD between the pre- and during-megadrought periods for all four sites (Table 2).

The two decades prior to the megadrought (1980–1999) showed a drying trend in certain months of the year at all four sites (Fig. 3a, d). The months of January, March, May, October, and November exhibited coherent drying trends in the form of increased atmospheric VPD. A trend towards reduced precipitation was revealed for January, March and September–December during these same decades. There were less clear trends toward a drier summer during the megadrought, except for decreasing precipitation in March (UAC and CCP) and April and October for (HEL, UAC, and GFP); however, the mean values during these periods were drier than those during the pre-megadrought period (Fig. 3c, f–h). As the megadrought emerged, the drier wintertime trends strengthened, especially in October and March. The wintertime VPD was higher during the post-2000 period

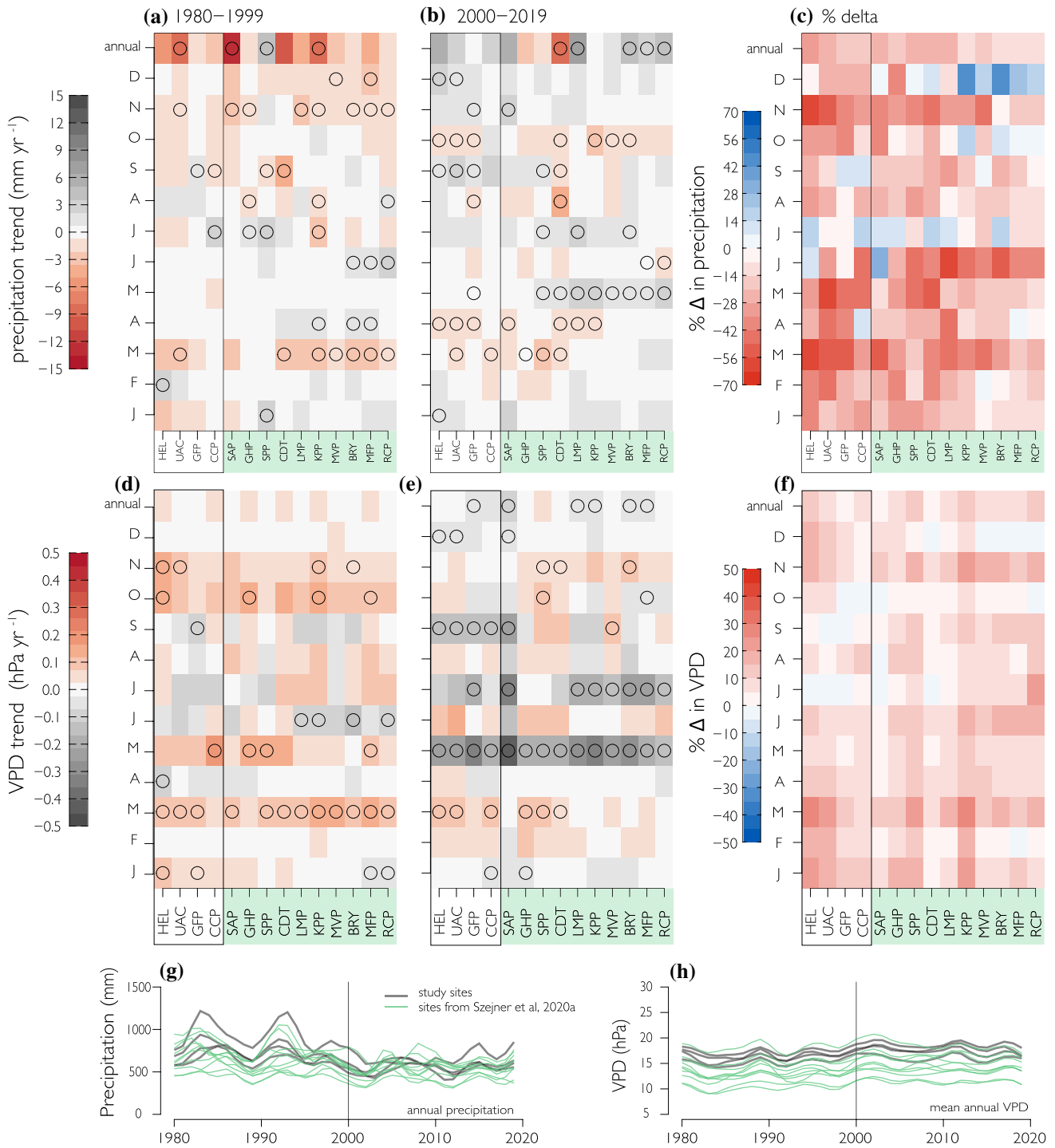


**Fig. 3** Trends in (a, b) monthly precipitation and (d, e) vapor pressure deficit for pre-2000 and post-2000, (c, f) percentage of change in the mean monthly values for each period, and (g, h) annual records in. Monthly data are from the PRISM database (PRISM Climate Group 2004). The color code in a, b, d, e shows the linear trends of precipitation in mm yr<sup>-1</sup> and of vapor pressure deficit in hPa yr<sup>-1</sup>. The color code in c, f shows the percentage of change between the mean values pre- and post-2000 such as:  $\% \text{delta} = \left( \bar{X}_{(2000-1999)} - \bar{X}_{(1980-1999)} \right) / \bar{X}_{(1980-1999)} \times 100$ . The x-axis

represents the sites and the y-axis represents the months. Circled spaces show statistically significant trends  $P < 0.05$ . The top row of each panel (labeled “annual”) shows the presence (or lack thereof) of any trend in precipitation or VPD for each site when evaluated for annual mean values during the 20-year timeframe covered by each panel. The sites with a green background or lines (g, h) are the ten reference sites from a larger tree-ring network drawn from a past study (Szejner et al. 2020a)

**Table 2** Difference of total precipitation (mm year<sup>-1</sup>) and vapor pressure deficit, VPD (hPa) between the two periods: 1980–1999 and 2000–2019 corresponding to pre- and post-onset of the megadrought for the four studies sites

Sites	Precipitation Difference (mm year <sup>-1</sup> )	Vapor pressure deficit Difference (hPa)
HEL	– 277.9*	1.71*
UAC	– 199.7*	1.32*
GFP	– 118.8*	0.79*
CCP	– 103.3*	0.85*

The statistical significance of the differences are shown as asterisks for all values, and were assessed using Mann–Whitney test at  $P < 0.05$

(Fig. 3f, h) at all four sites during most months and the largest difference was found in January, March and June, presumably due to the combined influences of atmospheric warming and reduced precipitation.

It is also evident from the ten additional (reference) sites located along the north–south NAM gradient (Szejner et al. 2020a, Fig. 3), that the pre-megadrought drying trend had been developing during the decades before 2000, indicating a regional phenomenon. Several months, mostly during the winter, showed significant drying trends in the period 1980–1999 at many of the reference sites (Fig. 3a, d). It is important to note that in some months (e.g., May) there were shallow trends revealing a slight increase in precipitation across years during the 2 decades of the megadrought (following 2000; Fig. 3b, e); but as stated earlier, an overall decrease in monthly average precipitation and an increase in monthly average VPD occurred during the megadrought (Table 2; Fig. 3c, f). It is also important to note that while all 14 sites showed decreases in mean precipitation and increases in mean VPD before and during the megadrought, the four southerly sites, considered separately from the ten reference sites, exhibited higher precipitation (due to the greater amounts of summer rain during the NAM) and higher VPD (due to higher air temperatures) (Fig. 3g, h). Thus, while there are some systematic and nuanced patterns in the nature of the drought, when considered across the entire Southwestern US, there is strong evidence that the development of a drier pre-megadrought period, and sustained overall deepening of the drought after 2000, was a regional event.

In this analysis, we decided to retain the autocorrelations that existed across seasons and years in the time series from all sites (see Szejner et al. 2018). We made this decision in the interest of using all the information captured within the time series that could possibly inform us about trends. There were cross-correlated interactions among climate and physiological processes that span seasons and years, and also contribute to predictive capabilities, which could have been lost if corrected for autocorrelation. However, we have also

evaluated the potential for autocorrelations within the climate (Tables S1 and S2) and isotope data (Fig. S3) to influence our conclusions. Using this supplementary data, we observed no significant autocorrelations in climate variables within any specified month at any of the four primary sites considered in this study. The correlations between  $\delta^{13}\text{C}$  and climate were less robust in the absence of time-dependent autocorrelation, but still significant at all four of the sites; though the trend for the IADF disappeared. The correlations with climate were generally weakened for  $\delta^{18}\text{O}$  in the EW signal, but retained in the LW signal. The predictive potential for RWI was weak and generally non-significant, for all sites combined, both with and without autocorrelation. Thus, we concluded that the correlations between  $\delta^{13}\text{C}$  and climate remain robust, even in the absence of autocorrelation, similar to the conclusions of Szejner et al. (2018), and correlations for  $\delta^{18}\text{O}$ -climate and RWI-climate remain weak in the absence of autocorrelations.

### Spatio-temporal trends of tree growth and stable isotopes

The time series for RWI and cellulose  $\delta^{13}\text{C}$  and  $\delta^{18}\text{O}$  are shown for individual ring components in Fig. 4. The two sites with the highest mean woody growth rates (UAC and CPP) showed significant progressive decreases in growth for both EW and LW for the 2-decade period leading up to 2000. The two other sites (HEL and GFP), which had slower-growing trees, showed either a smaller decrease in RWI trend, or no trend at all, leading up to the year 2000. These results are not influenced by potential tree age effects as trees were mature (age was  $\sim 100$  years) and we observed no significant difference in trends after removing any age effect from each sample (Fig. S6). During the fifteen-year period following 2000, tree growth at UAC remained suppressed at minimal values, whereas CPP showed recovery, even approaching pre-megadrought values. Growth increments in EW and LW for the HEL and GFP sites remained at pre-megadrought values throughout the megadrought period. Growth increments in the IADF were significantly lower than those for the EW and LW and showed only slightly negative trends or no trend at all (for three of the sites; CPP, GFP, and HEL). For trees at the UAC site, the IADF showed an apparent decrease in growth across the entire 30-year observation period, with a sharper decrease occurring after 2000.

An increasing trend in  $\delta^{13}\text{C}$  was evident across the entire 30-year observation period at all four sites and in all three-ring segments (EW, IADF, and LW). The one exception in this trend was for HEL LW, which did not increase. For the GFP and CPP sites, there was evidence of a relaxation trend at around 2007–2008—midway through the megadrought—and in all three-ring segments. For the  $\delta^{18}\text{O}$  chronologies,

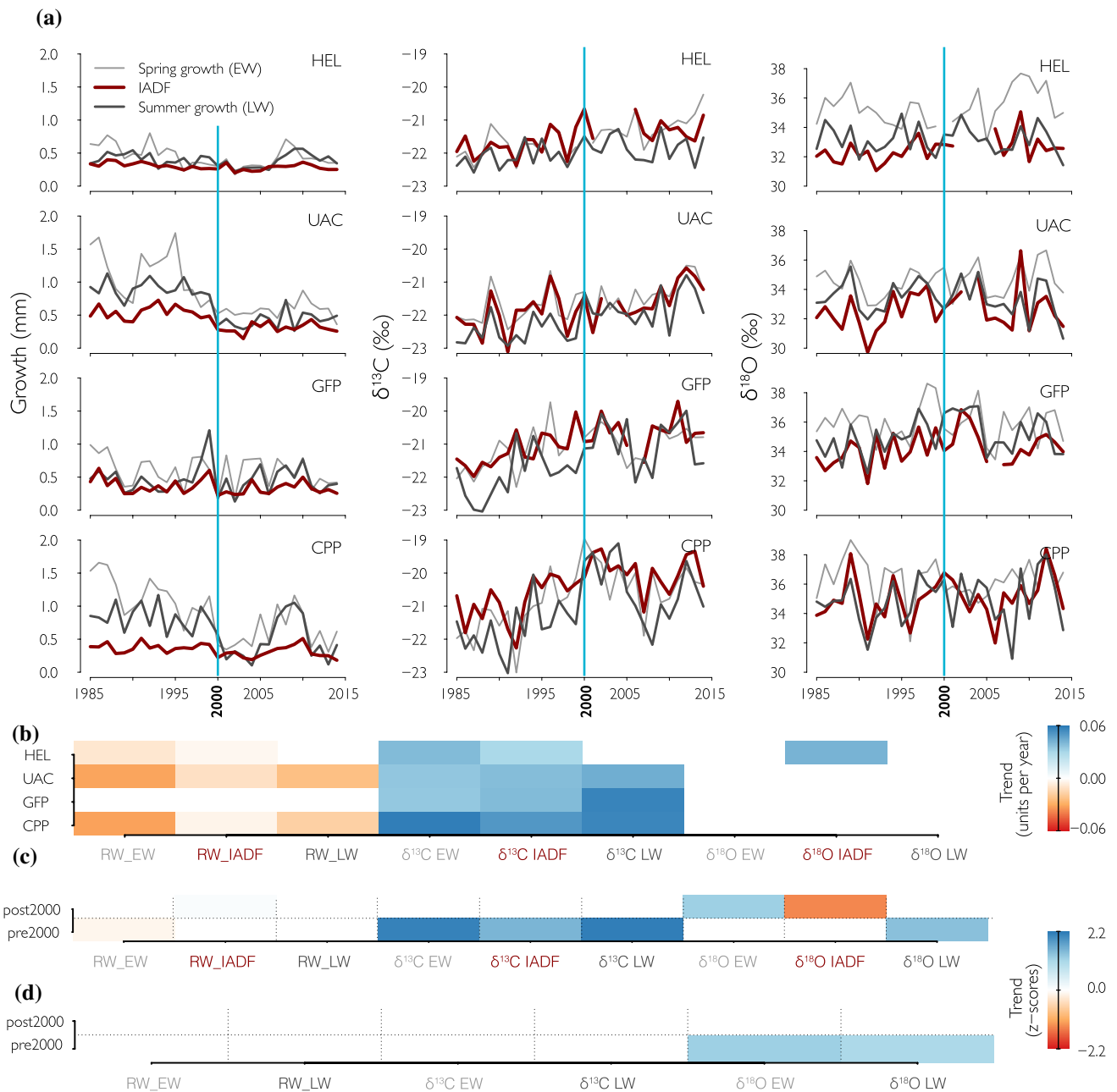


**Fig. 4** Variability in radial growth (mm),  $\delta^{13}\text{C}$  and  $\delta^{18}\text{O}$ . **a** Time series of earlywood (EW) is plotted in light grey lines, false latewood (or IADF) in red lines, and summer wood (SW) in dark grey lines. **b** Linear regression slopes (trends) against time of each parameter and for each site across the entire 30-year study period (1985–2014). Blue colors indicate significant and positive trends and orange colors show

significant and negative trends ( $P < 0.05$ ). **c** Pre-2000 and post-2000 rows show the trends after compositing the  $z$  scores for the four sites of this study. **d** Pre-2000 and post-2000 rows show the trends after compositing the  $z$  scores for the ten northerly (reference) sites from a previous study (Szejner et al. 2020a, b)

there were no apparent trends for the different subdivisions or sites, except for the HEL IADF chronology, which exhibited a positive trend. In all sites, the EW  $\delta^{18}\text{O}$  was more enriched compared to  $\delta^{18}\text{O}$  values of IADF and LW. For the HEL and UAC sites, the  $\delta^{18}\text{O}$  for IADF showed the lowest mean value and was most depleted in  $\delta^{18}\text{O}$ , compared to values from the EW and LW. For the GFP and CPP sites,

the  $\delta^{18}\text{O}$  of IADF and LW showed similar or overlapping mean values.

The lower boxes in Fig. 4 (panels b–d) show summarized trends in the isotope and RWI data. Trees in the four sites showed significant reductions in RWI and increases in  $\delta^{13}\text{C}$  when considered for the entire 30-year span of the study (Fig. 4b). When partitioned separately for the 15-year

period before and during the megadrought, the RWI trends disappeared (Fig. 4c). However, trends in  $\delta^{13}\text{C}$  were highly significant for the period before the megadrought in the EW, IADF, and LW fractions. For the ten reference sites, which were aligned along a latitudinal climate gradient, there were no significant trends in RWI or  $\delta^{13}\text{C}$  for the 2 decades prior to the megadrought (Fig. 4d). Although, interestingly, there were some slight trends toward increasing  $\delta^{18}\text{O}$ .

### Intra-seasonal profiles of growth and stable isotopes

The seasonal response within different portions of annual rings, including RWI and cellulose isotopes, for both pre- and post-2000, revealed transitions from the snowmelt-influenced spring period through the late-spring and early-summer arid period, and into the mid-summer monsoon period (Fig. 5). Generally, the bimodal precipitation pattern was recognized in high RWI growth in the EW fraction, minimal growth in the IADF (reflecting the arid period), and recovery to modest growth in the LW fraction. At almost all sites, EW1 and EW2 subdivisions had enriched  $\delta^{13}\text{C}$  and  $\delta^{18}\text{O}$  values, compared to the other ring fractions. The one exception was the CPP site, where the highest mean  $\delta^{13}\text{C}$  value was also found in the IADF. At all sites, the IADF showed depleted  $\delta^{18}\text{O}$  values compared to the previous EW subdivisions (except IADF  $\delta^{18}\text{O}$  in CPP), presumably reflecting the monsoon climate that occurs during IADF maturation (Belmecheri et al. 2018). The SW and LW fractions, which are both produced and matured after the hyper-arid period, showed reductions in both  $\delta^{13}\text{C}$  and  $\delta^{18}\text{O}$ , compared to the seasonal progression, reflecting the wetter and more humid conditions of the summer monsoon period.

The primary influence of the megadrought through reduced winter precipitation and increased spring VPD was observed in the significant difference between pre- and post-2000 in most of the sections in both RWI growth and  $\delta^{13}\text{C}$  (Fig. 5). There were some significant differences in greater EW growth reductions in the pre-2000 decade with the exception of GFP. With respect to  $\delta^{13}\text{C}$ , only the EW2 from GFP, did not show significant differences between the two periods. However, the  $\delta^{13}\text{C}$  and, therefore, the overall iWUE records for all five sub-divisions of annual rings were higher in during the megadrought, compared to before the megadrought.

## Discussion

Megadroughts, also known as multi-decadal droughts, are most commonly attributed to external forcings or internal instabilities and oscillations within the earth's climate system (Coats et al. 2016; Ault et al. 2018). Natural climate

cycles associated with the Eastern Pacific Ocean are the likely cause of the current southwestern megadrought, though there is good evidence that anthropogenic climate change has also contributed (Udall and Overpeck 2017; Williams et al. 2020). In general, megadroughts in the Western US are predicted at a frequency of 1–2 per millennium (Woodhouse and Overpeck 1998), so the current event is indeed a rare climatic occurrence. Models combined with a 1200-year tree-ring record have shown that the current megadrought is one of the fastest evolving and strongest multi-decadal droughts since the Medieval Era (Williams et al. 2020).

In our past studies we showed that the current megadrought is evident in both the winter and summer hydroclimate regimes (Szejner et al. 2020a). We further showed that the persistent and successive annual droughts, which compose the current megadrought, have caused cumulative stress in regional forests; rendering trees incapable of recovery from any single year's drought and exhibiting apparent multi-year legacy effects (Szejner et al. 2020a). Here, we have shown that the current megadrought was probably developing and influencing tree physiology since before its purported incipient year of 2000. Evidence of climate drying during the period 1980–1999 was apparent in the tree ecophysiological responses of *P. ponderosa* during specific months at the southernmost, arid portion of the species distribution range. The early stages of the megadrought were most evident in the trends for increasing cellulose  $\delta^{13}\text{C}$  values in most seasonal fractions of annual rings at all four study sites (Figs. 4 and 5). The trends were seen in the EW and IADF fractions. At the three easternmost sites, the trend was also evident in the later-summer fractions (which included SW and LW). The later-summer trend was not obvious at the westernmost site (HEL). The non-significant trend in the late-summer fractions of  $\delta^{13}\text{C}$  at HEL appears to be less due to relaxed drying during the megadrought, and more to reduced sensitivities during the pre-megadrought decades (Fig. 4b). The pre- and during-megadrought trends for the SW and LW  $\delta^{13}\text{C}$  fractions at this site deserve more study.

In contrast to the gradual increase in  $\delta^{13}\text{C}$ , starting before 2000, we observed no significant and consistent trends in  $\delta^{18}\text{O}$  (Fig. 4). This result was unexpected, as it is well known that  $\delta^{18}\text{O}$  isotope enrichment in leaf water should, according to theory, increase as VPD increases (Craig and Gordon 1965; Dongmann et al. 1974; Dawson and Ehleringer 1993), and there were clear increases in VPD from 1990 to 2019 (Fig. 3h). There is no reason to doubt that needle water  $^{18}\text{O}$  enrichment occurred throughout the megadrought, given the trends reported in Fig. 4 for  $\delta^{13}\text{C}$  and the associated VPD records. However, this expected trend was apparently not transferred to the cellulose  $\delta^{18}\text{O}$  composition of *P. ponderosa* tree rings. We offer three possible reasons for the

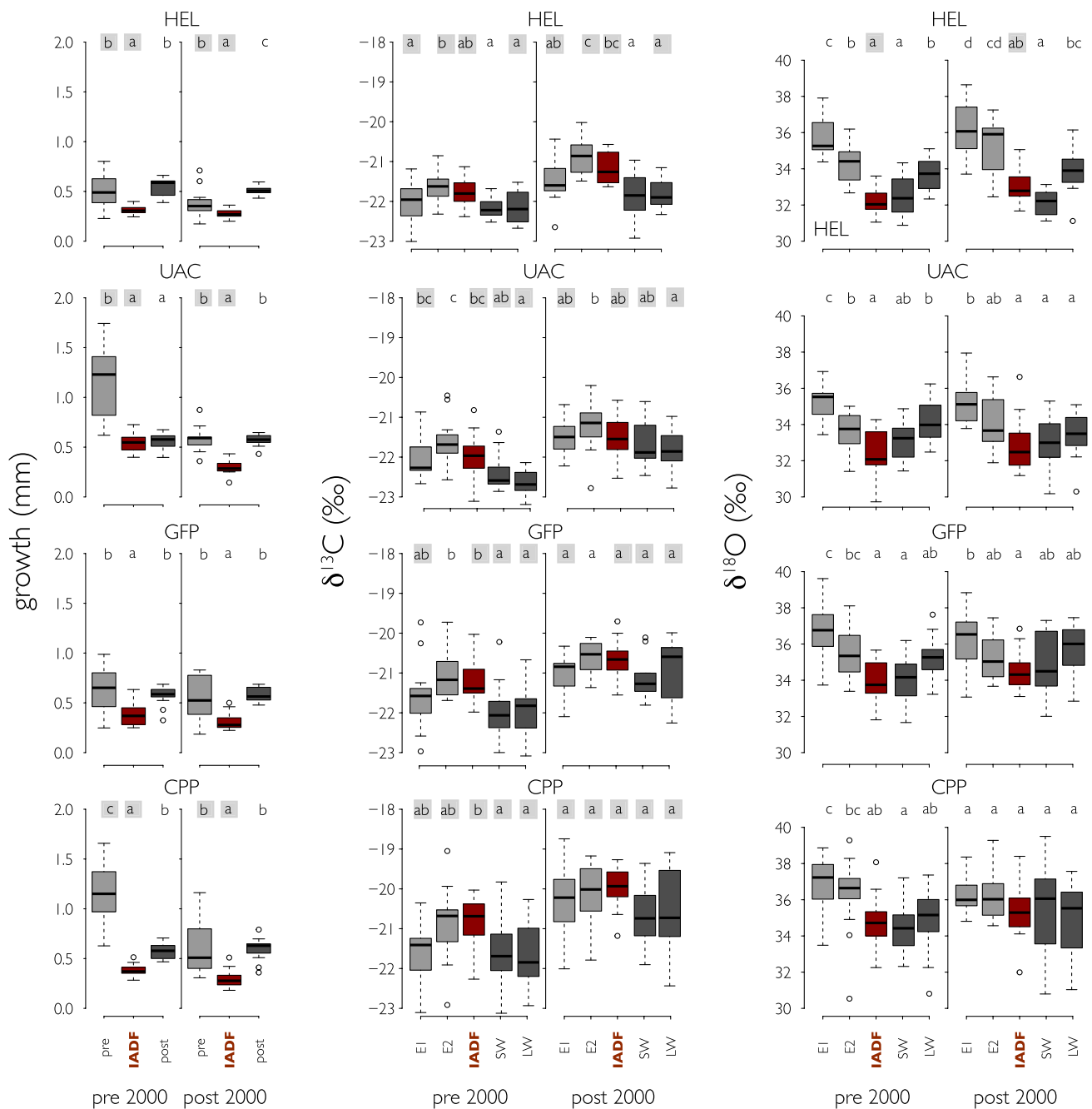


**Fig. 5** Boxplots of seasonal progression of RWI,  $\delta^{13}\text{C}$ , and  $\delta^{18}\text{O}$  for pre- and during-megadrought periods on different subsections of the rings, earlywood (pre, E1 and E2) in light grey, intra-annual density fluctuations (IADF) in red, summer wood (SW), and latewood (Post and LW) in dark grey. The letters at the top of each section indicate

the statistical significance between the mean of growth and isotopic values of each tree-ring subdivision. Subdivisions sharing the same letters are not significantly different from each other ( $P > 0.05$ ). The letters marked with a grey box indicate that difference between pre- and during-megadrought periods is significant different at  $P < 0.05$

lack of an observed  $\delta^{18}\text{O}$  trend. (1) There may have been a systematic change in source-water  $\delta^{18}\text{O}$  values. Climate changes to the west of our study sites may have caused a shift in the  $\delta^{18}\text{O}$  of meteoric water due to Rayleigh-type fractionations as air masses from the Pacific Coast moved eastward, rising over the Sierra Nevada Mountains, and

descending to the arid Southwestern US. During the period 1990–2007, which includes periods before and after the megadrought, winter rainfall amount progressively declined at Tucson, Arizona (near the western edge of our study area and the HEL site), which is consistent with the precipitation trends that we report here, but with no change in mean  $\delta^{18}\text{O}$

(Eastoe and Dettman 2016). Mean summer rainfall amounts and  $\delta^{18}\text{O}$  ratios for the Tucson record were both unchanged during this same period (Eastoe and Dettman 2016). Based on these observations, there appears to be no support for our first hypothesis. (2) Increased drought may have caused an increase in the opportunities for exchanges in the oxygen isotopes from source water and cambial sugar substrates during cellulose synthesis, often referred to as  $P_{\text{ex}}$  (Hill et al. 1995; Barbour 2007; Szejner et al. 2020b). This exchange provides an opportunity for a post-assimilation and it works in the direction of opposing evaporative isotope enrichment during photosynthesis in the needles (Gessler et al. 2014; Song et al. 2014). In a past study with Australian eucalypts, Cheesman and Cernusak (2017) estimated that  $P_{\text{ex}}$  increased at the driest sites along an aridity gradient. They hypothesized that this is due to drought-related increases in the turnover time of carbohydrates and concomitantly, the frequency of secondary oxygen exchanges (sensu Song et al. 2014). It is possible that the progressive decadal-scale increases in drought, in sites with *P. ponderosa*, has a similar effect on  $P_{\text{ex}}$ . However, at this time, there is so little known about the relationships among sugar cycling, oxygen isotope exchange and drought in forest trees, that it would be premature to accept or reject changes in  $P_{\text{ex}}$  as an explanation for the lack of sensitivity in  $\delta^{18}\text{O}$  at our sites. (3) Recent research has shown that the evaporative enrichment of needle water with  $^{18}\text{O}$  in two pine species, including *P. ponderosa*, progressively increases from base to tip (Kannenberget al. 2021). It has also been shown that progressive  $^{18}\text{O}$  enrichment along *P. ponderosa* needles increases the uncoupling of needle and phloem sugar  $\delta^{18}\text{O}$ , attenuating the original evaporation signal recorded at the time of  $\text{CO}_2$  assimilation. This is a third possible explanation for the absence of clear  $\delta^{18}\text{O}$ -climate correlations at our study sites. It is not likely that the effect of progressive enrichment can completely obscure the evaporative fractionation originally recorded at the time of  $\text{CO}_2$  assimilation. However, it is likely to reduce the variance, making it more challenging to discern tree-ring  $\delta^{18}\text{O}$ -climate relations (Figs. S4, S5). Once again, this hypothesis is too recent and not tested widely enough to invoke it as an explanation for the lack of multi-decadal  $\delta^{18}\text{O}$  trends at our study sites, but it does provide one additional possibility for future exploration.

Although we found no clear trends in  $\delta^{18}\text{O}$  across multiple years, we did observe evidence for seasonal dynamics in  $\delta^{18}\text{O}$  that reflected correlations with precipitation and VPD in all the different annual ring fractions (Fig. S4). EW cellulose generally showed higher  $\delta^{18}\text{O}$  enrichment, presumably reflecting the high evaporative potential of late-spring and early-summer droughts. Maturation of EW tracheids is generally offset from cambial production by several weeks (Belmecheri et al. 2018; Morino et al. 2021), meaning that cellulose is added to secondary cell walls in the late spring, and

even continuing into the early-summer hyper-arid period. Similarly, the narrow diameter of IADF cells, which follow the EW and reflect the hyper-arid period, mature later in the summer, after initiation of NAM rains. Thus, the anatomical and stable isotope features of the IADF reflect processes that are seasonally and hydrologically uncoupled from one another (Belmecheri et al. 2018). We observed that the  $\delta^{18}\text{O}$  recorded in the IADF is lower in all cases, compared to the EW (Figs. 4 and 5). If correct, this explanation would require a relaxation in evaporative enrichment of needle sugars in response to lower VPD during the later-summer NAM period, compared to the hyper-arid period; which is reasonable and consistent with theory. It is possible that the lower  $\delta^{18}\text{O}$  values of the IADF are due to an increase in  $P_{\text{ex}}$ , during the later-summer NAM period, compared to the hyper-arid period. However, we have no observations of seasonal variations in the source water, and it is more likely that the  $\delta^{18}\text{O}$  of the source water is increased, not decreased, relative to earlier-season source water (Eastoe and Dettman 2016). Thus, it is most likely that seasonally offset cambial phenology between tracheid formation and maturation explains the discordant anatomical and isotope results. Such results are further supported by proxy forward modelling of cellulose  $^{18}\text{O}$  in one of the studied sites (HEL). The modelled intra-seasonal variations and isotopic amplitude of cellulose  $^{18}\text{O}$  were better explained by intra-seasonal variability of VPD and offsets in the timing of tracheid formation versus maturation, compared to source water variations (Belmecheri et al. 2018).

An explanation for the increase in  $\delta^{13}\text{C}$  in the SW and LW fractions of the annual rings, despite weak and geographically restricted trends in reduced precipitation and VPD during the summer months, in both the pre- and post-2000 periods are not explained through direct interactions between climate and carbon-isotope fractionation processes. Past studies in *P. ponderosa* have shown cross-correlations between EW and LW  $\delta^{13}\text{C}$  values, suggesting that cross-seasonal physiological linkages (use of stored carbohydrates from earlier in the season) are relevant (Szejner et al. 2018). Similar linkages may be present in this study, although we chose trees with clear IADFs that separated the PRE- and POST-seasonal processes. The presence of the IADF, in theory, indicates that cambial activity is reset after the hyper-arid period, and before the mid-to-late season monsoon activity, which should cause the isotopic signatures of POST-tree-ring fractions to be uncoupled from the early-season and hyper-arid hydroclimates, and their associated PRE-tree-ring fractions (see de Luis et al. 2011). This may not be the case in *P. ponderosa* trees from the four sites that we studied. It is possible that common pools of carbohydrates—with similar isotopic compositions—were used for cambial growth both before and after the hyper-arid period,

allowing for cross-seasonal correlation in  $\delta^{13}\text{C}$  (Figs. S1, S2; also see Szejner et al. 2018).

The foreshadowing of megadrought conditions that we detected in the  $\delta^{13}\text{C}$  data, especially during the 1990–1999 decade, was not an inherent tree property, but rather an interaction between tree physiology and a subtle shift in the climate system at the arid boundary for species distribution. The shift included decadal-scale drying trends that slowly manifested during certain months of the autumn and winter (Fig. 3). In other words, the megadrought did not occur as a sharply defined shift in the climate system, but rather as a decadal-long, seasonally disparate and stochastic drying trend that gradually coalesced into an organized climate episode and increased in intensity after 2000. This pattern is particularly clear in the precipitation data of Fig. 3, where the pre-2000 period (Fig. 3a) shows drying trends in January, March, June, and September–November, but not in many of the adjacent months. After 2000, as shown in the panels on the right (Fig. 3c, g), the drying trends were relaxed in several months, but the mean total amount of precipitation settled into a deepening deficit, relative to the long-term mean—being between 29 and 17% lower than mean precipitation values and the VPD remained at least 11–5% higher compared to previous decades (Fig. 3c, f–h). The sum of these trends shows that the climate at these southern sites, during the decades preceding the megadrought, included numerous opportunities for the physiological forcing of higher  $\delta^{13}\text{C}$  values in *P. ponderosa*, which were then sustained during the succeeding decades of the megadrought.

The physiological sensitivity of trees at the four southern sites to scattered drying trends before the megadrought, was not observed in trees further north, within the core range of the species. In the past study by Szejner et al. (2020a), trees from ten sites along a north–south axis through the megadrought domain, and well within the core range of *P. ponderosa*, showed no evidence of systematic increases in  $\delta^{13}\text{C}$  for EW or LW during the decades prior to 2000 (also Fig. 4d). This is despite the fact that the climate data showed similar megadrought conditions through the entire southwestern domain represented by the ten reference sites, compared to the southern sites (Fig. 3). Our analysis revealed that it is the trend in increasing ‘sensitivity’ to drought at the four southern sites that is most distinct. Our results show that the unique behavior of trees at the southern sites is not only distinguished across geographic space, but also across the multi-decadal time scale.

Our study provides correlational evidence that climate drying trends in the decades prior to the emergent megadrought are predicted by tree responses, particularly in the  $\delta^{13}\text{C}$  values of tree-ring cellulose. We do not have insight into the exact variable, or combination of variables, that drive the trends in sensitivity. It is likely that there are multivariate influences involved in the observed trends,

including several internal, physiological processes (Gessler et al. 2014). Factors such as fractionation associated with the loading of sugars into phloem and the use of stored carbon sources for cellulose synthesis can decouple  $\delta^{13}\text{C}$  values from the climate influences recorded during  $\text{CO}_2$  assimilation. It will require further study within a multivariate context, and separating systematic and random components of the trends to truly grasp the underlying causes of the trends we observed.

In this study, we provided data on the tree-ring stable isotope composition and ring-width growth trends in *P. ponderosa* trees from four sites, which are geographically separated from those used in past transects that we have studied (Szejner et al. 2016, 2018, 2020a). The new sites are aligned in a relatively narrow latitudinal band, unlike sites from the previous studies. The four new sites were situated at the southern, most arid limit of *P. ponderosa*. A related pine, *Pinus arizonica* var. *arizonica*, extends further south, into the Chihuahuan region of Mexico, and is capable of hybridization with *P. ponderosa*; but, *P. ponderosa*, as a distinct species, is limited in its southern extent to the region of the four populations that we studied (Shinneman et al. 2016). The fact that we observed a sustained physiological response to pre-megadrought drying trends in these southern sites, but not in the northern sites of the previous studies, suggests a different physiological constitution in trees near their arid niche limit. We hypothesize that the four southern sites are exposed to scattered drying trends during key months in the winter in the decades leading up to the formal start of the megadrought. It is also likely that populations of *P. ponderosa* in these southern sites have been exposed to past selection regimes that enhance tree sensitivity to drought and permit needle carbon and water cycling to be more tightly coupled to drought dynamics. The combination of drying trends and greater evolved sensitivity in the trees, is likely to produce the foreshadowing of the megadrought in  $\delta^{13}\text{C}$  in tree rings that we observed in this study using intra-annual measurements. An understanding of such early indicators in sub-annual  $\delta^{13}\text{C}$  records in the tree rings of semi-arid montane conifers could be useful in future forest management efforts, providing data for both strategic decisions and for the conditioning of prognostic models used to predict drought threats. As the 2000–2020 megadrought continues to unfold, it will be of interest to reassess future patterns of tree responses, especially in widespread montane species, such as *P. ponderosa*.

**Supplementary Information** The online version contains supplementary material available at <https://doi.org/10.1007/s00442-021-04916-9>.

**Acknowledgements** This manuscript is to be published as part of a Special Issue honoring Russell K. Monson. We appreciate particularly Russ’ extensive contributions in plant ecology. We also thank C. Niel, A. Thomas, L. Wells, F. Moreno, M. Twitty, A. Spencer, C.

Monteleone, and E. Bergman for their assistance in blue reflectance tree-ring and cellulose sample processing. This work was supported by a grant from the Ecosystems Program in the Division of Environmental Biology (NSF Award 1754430). FB acknowledges support from project 'Inside out' (#POIR.04.04.00-00-5F85/18-00) funded by the HOMING program of the Foundation for Polish Science co-financed by the European Union under the European Regional Development Fund.

**Author contribution statement** WEW, SB, FB, PS, and RKM conceived the ideas and designed methodology. PS, SB, and WEW collected the data. PS, SB, and FB analyzed the data. PS and RKM led the writing of the manuscript. All authors contributed critically to the drafts and gave final approval for publication.

**Data accessibility** All data for this manuscript will be posted in the International Tree-Ring Database (ITRDB).

## Declarations

**Conflict of interest** The authors declare that they have no conflict of interest.

## References

- Acosta-Hernández AC, Julio Camarero J, Pompa-García M (2019) Seasonal growth responses to climate in wet and dry conifer forests. *IAWA J* 40:311–330. <https://doi.org/10.1163/22941932-40190226>
- Ault TR, StGeorge S, Smerdon JE, Coats S, Mankin JS, Carrillo CM, Cook BI, Stevenson S (2018) A robust null hypothesis for the potential causes of megadrought in Western North America. *J Clim* 31(1):3–24
- Babst F, Wright WE, Szejner P, Wells L, Belmecheri S, Monson RK (2016) Blue intensity parameters derived from ponderosa pine tree rings characterize intra-annual density fluctuations and reveal seasonally divergent water limitations. *Trees-Struct Funct* 30:1403–1415. <https://doi.org/10.1007/s00468-016-1377-6>
- Barbour MM (2007) Stable oxygen isotope composition of plant tissue: a review. *Funct Plant Biol* 34:83–94. <https://doi.org/10.1071/FP06228>
- Battipaglia G, Campelo F, Vieira J, Grabner M, De Micco V, Nabais C, Cherubini P, Carrer M, Bräuning A, Čufar K, Di Filippo A, García-González I, Koprowski M, Klisz M, Kirilyanov AV, Zafirov N, de Luis M, Cherubin P, Carrer M (2016) Structure and function of intra-annual density fluctuations: mind the gaps. *Front Plant Sci* 7:1–8. <https://doi.org/10.3389/fpls.2016.00595>
- Belmecheri S, Wright WE, Szejner P, Morino KA, Monson RK (2018) Carbon and oxygen isotope fractionations in tree rings reveal interactions between cambial phenology and seasonal climate. *Plant Cell Environ* 41:2758–2772. <https://doi.org/10.1111/pce.13401>
- Borchers HW (2019) R package “pracma”: practical numerical math functions
- Budelsky CA (1969) Variation in transpiration and its relationship with growth for *Pinus ponderosa* Lawson in Southern Arizona. University of Arizona
- Campbell R, McCarroll D, Robertson I, Loader NJ, Grudd H, Gunnarson B (2011) Blue intensity in *Pinus sylvestris* tree rings: a manual for a new palaeoclimate proxy. *Tree-Ring Res* 67:127–134. <https://doi.org/10.3959/2010-13.1>
- Cheesman AW, Cernusak LA (2017) Infidelity in the outback: climate signal recorded in  $\Delta^{18}\text{O}$  of leaf but not branch cellulose of eucalypts across an Australian aridity gradient. *Tree Physiol* 37:554–564. <https://doi.org/10.1093/treephys/tpw121>
- Coats S, Smerdon JE, Karnauskas KB, Seager R (2016) The improbable but unexceptional occurrence of megadrought clustering in the American West during the medieval climate anomaly. *Environ Res Lett* 11:074025. <https://doi.org/10.1088/1748-9326/11/7/074025>
- Cook BI, Seager R (2013) The response of the North American monsoon to increased greenhouse gas forcing. *J Geophys Res Atmos* 118:1690–1699. <https://doi.org/10.1002/jgrd.50111>
- Cook ER, Meko DM, Stahle DW, Cleaveland MK (1999) Drought reconstructions for the continental United States\*. *J Clim* 12:1145–1162. [https://doi.org/10.1175/1520-0442\(1999\)012%3c1145:DRFTCU%3e2.0.CO;2](https://doi.org/10.1175/1520-0442(1999)012%3c1145:DRFTCU%3e2.0.CO;2)
- Cook ER, Seager R, Heim RR, Vose RS, Herweijer C, Woodhouse C (2010) Megadroughts in North America: placing IPCC projections of hydroclimatic change in a long-term palaeoclimate context. *J Quat Sci* 25:48–61. <https://doi.org/10.1002/jqs.1303>
- Craig H, Gordon L (1965) Deuterium and oxygen 18 variations in the ocean and the marine atmosphere. In: Tongiorgi E (ed) Stable isotopes in oceanographic studies and paleotemperatures. Consiglio Nazionale delle ricerche Laboratorio di Geologia Nucleare, Pisa, pp 9–130
- Dawson TE, Ehleringer JR (1993) Isotopic enrichment of water in the “woody” tissues of plants: implications for plant water source, water uptake, and other studies which use the stable isotopic composition of cellulose. *Geochim Cosmochim Acta* 57:3487–3492. [https://doi.org/10.1016/0016-7037\(93\)90554-A](https://doi.org/10.1016/0016-7037(93)90554-A)
- de Luis M, Novak K, Raventós J, Gričar J, Prislán P, Čufar K (2011) Climate factors promoting intra-annual density fluctuations in aleppo pine (*Pinus halepensis*) from semiarid sites. *Dendrochronologia* 29:163–169. <https://doi.org/10.1016/j.dendro.2011.01.005>
- De Micco V, Saurer M, Aronne G, Tognetti R, Cherubini P (2007) Variations of wood anatomy and  $\delta^{13}\text{C}$  within-tree rings of coastal *Pinus pinaster* showing intra-annual density fluctuations. *IAWA J* 28:61–74. <https://doi.org/10.1163/22941932-90001619>
- Dongmann G, Nürnberg HW, Förstel H, Wagener K (1974) On the enrichment of  $\text{H}_2^{18}\text{O}$  in the leaves of transpiring plants. *Radiat Environ Biophys* 11:41–52. <https://doi.org/10.1007/BF01323099>
- Eastoe CJ, Dettman DL (2016) Isotope amount effects in hydrologic and climate reconstructions of monsoon climates: implications of some long-term data sets for precipitation. *Chem Geol* 430:78–89. <https://doi.org/10.1016/j.chemgeo.2016.03.022>
- Ehleringer JR, Cerling TE (1995) Atmospheric  $\text{CO}_2$  and the ratio of intercellular to ambient  $\text{CO}_2$  concentrations in plants. *Tree Physiol* 15:105–111. <https://doi.org/10.1093/treephys/15.2.105>
- Evans MN, Reichert BK, Kaplan A, Anchukaitis KJ, Vaganov EA, Hughes MK, Cane MA (2006) A forward modeling approach to paleoclimatic interpretation of tree-ring data. *J Geophys Res Biogeosci* 111:1–13. <https://doi.org/10.1029/2006JG000166>
- Farquhar GD, O'Leary MH, Berry JA (1982) On the relationship between carbon isotope discrimination and the intercellular carbon-dioxide concentration in leaves. *Aust J Plant Physiol* 9:121–137
- Francey R, Farquhar G (1982) An explanation of  $^{13}\text{C}/^{12}\text{C}$  variations in tree rings. *Nature* 297:28–31
- Frank DC, Poulter B, Saurer M, Esper J, Huntingford C, Helle G, Treyde K, Zimmermann NE, Schleser GH, Ahlström A, Ciais P, Friedlingstein P, Levis S, Lomas M, Sitch S, Viovy N, Andreu-Hayles L, Bednarz Z, Berninger F (2015) Water-use efficiency and transpiration across European forests during the Anthropocene. *Nat Clim Chang* 5:579–583. <https://doi.org/10.1038/nclimate2614>
- Fritts H (1976) Tree rings and climate. Academic P. Elsevier
- Fritts HC, Vaganov EA, Sviderskaya IV, Shashkin AV (1991) Climatic variation and tree-ring structure in conifers: empirical and mechanistic models of tree-ring width, number of cells, cell size,

- cell-wall thickness and wood density. *Clim Res* 1:97–116. <https://doi.org/10.3354/cr001097>
- Gessler A, Ferrio JP, Hommel R, Treydte K, Werner R, a, Monson RK, (2014) Stable isotopes in tree rings: towards a mechanistic understanding of isotope fractionation and mixing processes from the leaves to the wood. *Tree Physiol* 34:796–818. <https://doi.org/10.1093/treephys/tpu040>
- Green JW (1963) Wood cellulose. In: Whistler RL (ed) *Methods in carbohydrate chemistry*, vol 3. Academic Press, New York, pp 9–21
- Griffin D, Meko DM, Touchan R, Leavitt SW, Woodhouse CA (2011) Latewood chronology development for summer-moisture reconstruction in the US Southwest. *Tree-Ring Res* 67:87–101. <https://doi.org/10.3959/2011-4.1>
- Higgins RW, Yao Y, Wang XL (1997) Influence of the North American monsoon system on the U.S. summer precipitation regime. *J Clim* 10:2600–2622. [https://doi.org/10.1175/1520-0442\(1997\)010%3c2600:IOTNAM%3e2.0.CO;2](https://doi.org/10.1175/1520-0442(1997)010%3c2600:IOTNAM%3e2.0.CO;2)
- Hill SA, Waterhouse JS, Field EM, Switsur VR, Ap Rees T (1995) Rapid recycling of triose phosphates in oak stem tissue. *Plant Cell Environ* 18:931–936. <https://doi.org/10.1111/j.1365-3040.1995.tb00603.x>
- Holmes RL (1992) *Dendrochronology program library, instruction and program manual* (January 1992 update)
- Kannenber SA, Fiorella RP, Anderegg WRL, Monson RK, Ehleringer JR (2021) Seasonal and diurnal trends in progressive isotope enrichment along needles in two pine species. *Plant Cell Environ* 44:143–155. <https://doi.org/10.1111/pce.13915>
- Keeling CD, Piper SC, Bacastow RB, Wahlen M, Whorf TP, Heimann M, Meijer HA (2005) Atmospheric CO<sub>2</sub> and <sup>13</sup>CO<sub>2</sub> exchange with the terrestrial biosphere and oceans from 1978 to 2000: observations and carbon cycle implications. In: Baldwin I et al (eds) *A history of atmospheric CO<sub>2</sub> and its effects on plants, animals, and ecosystems*. Springer-Verlag, New York, pp 83–113
- Knowles JF, Molotch NP, Trujillo E, Litvak ME (2018) Snowmelt-driven trade-offs between early and late season productivity negatively impact forest carbon uptake during drought. *Geophys Res Lett* 45:3087–3096. <https://doi.org/10.1002/2017GL076504>
- Knowles JF, Scott RL, Minor RL, Barron-Gafford GA (2020) Ecosystem carbon and water cycling from a sky island montane forest. *Agric For Meteorol* 281:107835. <https://doi.org/10.1016/j.agrfor.2019.107835>
- Laumer W, Andreu L, Helle G, Schleser GH, Wieloch T, Wissel H (2009) A novel approach for the homogenization of cellulose to use micro-amounts for stable isotope analyses. *Rapid Commun Mass Spectrom* 23:1934–1940. <https://doi.org/10.1002/rcm.4105>
- Leavitt SW, Danzer SR (1993) Method for batch processing small wood samples to holocellulose for stable-carbon isotope analysis. *Anal Chem* 65:87–89. <https://doi.org/10.1021/ac00049a017>
- Leavitt SW, Wright WE, Long A (2002) Spatial expression of ENSO, drought, and summer monsoon in seasonal δ<sup>13</sup>C of ponderosa pine tree rings in southern Arizona and New Mexico. *J Geophys Res* 107:4349. <https://doi.org/10.1029/2001JD001312>
- Leavitt SW, Woodhouse CA, Castro CL, Wright WE, Meko DM, Touchan R, Griffin D, Ciancarelli B (2011) The North American monsoon in the U.S. Southwest: potential for investigation with tree-ring carbon isotopes. *Quat Int* 235:101–107. <https://doi.org/10.1016/j.quaint.2010.05.006>
- McCarroll D, Gagen MH, Loader NJ, Robertson I, Anchukaitis KJ, Los S, Young GHF, Jalkanen R, Kirchhefer A, Waterhouse JS (2009) Correction of tree ring stable carbon isotope chronologies for changes in the carbon dioxide content of the atmosphere. *Geochim Cosmochim Acta* 73:1539–1547. <https://doi.org/10.1016/j.gca.2008.11.041>
- Monson RK, Turnipseed AA, Sparks JP, Harley PC, Scott-Denton LE, Sparks K, Huxman TE (2002) Carbon sequestration in a high-elevation, subalpine forest. *Glob Chang Biol* 8:459–478. <https://doi.org/10.1046/j.1365-2486.2002.00480.x>
- Monson RK, Szejner P, Belmecheri S, Morino KA, Wright WE (2018) Finding the seasons in tree ring stable isotope ratios. *Am J Bot* 105:1–3. <https://doi.org/10.1002/ajb2.1083>
- Morino K, Minor RL, Barron-Gafford GA, Brown PM, Hughes MK (2021) Bimodal cambial activity and false-ring formation in conifers under a monsoon climate. *Tree Physiol*. <https://doi.org/10.1093/treephys/tpab045>
- Pacheco A, Camarero JJ, Pompa-García M, Battipaglia G, Voltas J, Carrer M (2019) Growth, wood anatomy and stable isotopes show species-specific couplings in three Mexican conifers inhabiting drought-prone areas. *Sci Total Environ* 5:134055. <https://doi.org/10.1016/j.scitotenv.2019.134055>
- PRISM\_Climate\_group (2004) Oregon State University. In: *Prism*. <http://prism.oregonstate.edu>. Accessed 2019
- Roden J, Lin G, Ehleringer JR (2000) A mechanistic model for interpretation of hydrogen and oxygen isotope ratios in tree-ring cellulose. *Geochim Cosmochim Acta* 64:21–35. [https://doi.org/10.1016/S0016-7037\(99\)00195-7](https://doi.org/10.1016/S0016-7037(99)00195-7)
- Shinneman DJ, Means RE, Potter KM, Hipkins VD (2016) Exploring climate niches of ponderosa pine (*Pinus ponderosa* Douglas ex Lawson) haplotypes in the Western United States: implications for evolutionary history and conservation. *PLoS ONE* 11:e0151811. <https://doi.org/10.1371/journal.pone.0151811>
- Song X, Farquhar GD, Gessler A, Barbour MM (2014) Turnover time of the non-structural carbohydrate pool influences δ<sup>18</sup>O of leaf cellulose. *Plant Cell Environ* 37:2500–2507. <https://doi.org/10.1111/pce.12309>
- Stahle DW, Cook ER, Burnette DJ, Torbenson MCA, Howard IM, Griffin D, Diaz JV, Cook BI, Williams AP, Watson E, Sauchyn DJ, Pederson N, Woodhouse CA, Pederson GT, Meko D, Coulthard B, Crawford CJ (2020) Dynamics, variability, and change in seasonal precipitation reconstructions for North America. *J Clim* 33:3173–3195. <https://doi.org/10.1175/jcli-d-19-0270.1>
- Stokes MA, Smiley TL (1996) *An introduction to tree-ring dating*. The University of Arizona Press, Tucson
- Szejner P, Wright WE, Babst F, Belmecheri S, Trouet V, Leavitt SW, Ehleringer JR, Monson RK (2016) Latitudinal gradients in tree ring stable carbon and oxygen isotopes reveal differential climate influences of the North American monsoon system. *J Geophys Res Biogeosci* 121:1978–1991. <https://doi.org/10.1002/2016JG003460>
- Szejner P, Wright WE, Belmecheri S, Meko D, Leavitt SW, Ehleringer JR, Monson RK (2018) Disentangling seasonal and interannual legacies from inferred patterns of forest water and carbon cycling using tree-ring stable isotopes. *Glob Chang Biol* 24:5332–5347. <https://doi.org/10.1111/gcb.14395>
- Szejner P, Belmecheri S, Ehleringer JR, Monson RK (2020a) Recent increases in drought frequency cause observed multi-year drought legacies in the tree rings of semi-arid forests. *Oecologia* 192:241–259. <https://doi.org/10.1007/s00442-019-04550-6>
- Szejner P, Clute T, Anderson E, Evans MN, Hu J (2020b) Reduction in lumen area is associated with the δ<sup>18</sup>O exchange between sugars and source water during cellulose synthesis. *New Phytol* 226:1583–1593. <https://doi.org/10.1111/nph.16484>
- Treydte K, Boda S, Graf Pannatier E, Fonti P, Frank D, Ullrich B, Saurer M, Siegwolf R, Battipaglia G, Werner W, Gessler A (2014) Seasonal transfer of oxygen isotopes from precipitation and soil to the tree ring: source water versus needle water enrichment. *New Phytol* 202:772–783. <https://doi.org/10.1111/nph.12741>
- Udall C, Overpeck J (2017) The twenty-first century Colorado River hot drought and implications for the future. *Water Resour Res* 53:2404–2418. <https://doi.org/10.1002/2016WR019638>
- Williams AP, Cook ER, Smerdon JE, Cook BI, Abatzoglou JT, Bolles K, Baek SH, Badger AM, Livneh B (2020) Large contribution

- from anthropogenic warming to an emerging North American megadrought. *Science* 368:314–318. <https://doi.org/10.1126/science.aaz9600>
- Woodhouse CA, Overpeck JT (1998) 2000 years of drought variability in the central United States. *Bull Am Meteorol Soc* 79:2693–2714
- Zalloni E, de Luis M, Campelo F, Novak K, De Micco V, Di Filippo A, Vieira J, Nabais C, Rozas V, Battipaglia G (2016) Climatic signals from intra-annual density fluctuation frequency in Mediterranean pines at a regional scale. *Front Plant Sci* 7:579. <https://doi.org/10.3389/fpls.2016.00579>